Front. Earth Sci. 2019, 13(2): 303–316
https://doi.org/10.1007/s11707-018-0746-4

RESEARCH ARTICLE

Effects of sea level rise on storm surge and waves within the Yangtze River Estuary

Yongming SHEN (✉)[1,2], Gefei DENG[1], Zhihao XU[3], Jun TANG[1]

1 State Key Laboratory of Coastal and Offshore Engineering, Dalian University of Technology, Dalian 116024, China
2 Institute of Environmental and Ecological Engineering, Guangdong University of Technology, Guangzhou 510006, China
3 Research Center for Eco-Environmental Engineering, Dongguan University of Technology, Dongguan 523808, China

Abstract Sea level rise (SLR) can cause water depth increase (WDI) and coastal inundation (CI). By applying the coupled FVCOM + SWAN model, this study investigates the potential impacts of WDI and CI, induced by a 1.0 m SLR, on storm surge and waves within the Yangtze River Estuary. A 1.0 m WDI decreases the maximum storm surge by 0.15 m and increases the maximum significant wave height by 0.35 m. The CI effect size is smaller when compared with WDI. CI decreases the maximum storm surge and significant wave height by 0.04 and 0.07 m, respectively. In the near-shore area, WDI significantly alters the local hydrodynamic environment, thereby stimulating changes in maximum storm surges and wave heights. Low-lying regions are negatively impacted by CI. Conversely, in deep-water areas, the relative change in water depth is minimal and the effect of CI is gradually enhanced. The combined effect of WDI and CI decreases the maximum surge by 0.31 m and increases the maximum significant wave height by 0.21 m. As a result, CI may be neglected when designing deep-water infrastructures. Nonetheless, the complex interactions between adoption and neglect of CI should be simulated to achieve the best seawall flood control standards and design parameters.

Keywords sea level rise, FVCOM + SWAN, coastal inundation, Yangtze River Estuary

1 Introduction

Low-lying coastal cities are vulnerable to storm surges caused by tropical cyclones, such as Haikui (2012), Haiyan (2013), and Muifa (2017). According to the China Marine Disaster Bulletin, annual average economic losses resulting from typhoons and storm surges were estimated at $1.6 billion for the period 2012–2016 (Wang et al., 2018). About 10% of the world's population lives in coastal zones below 10 m in elevation, which cover only 2% of the world's land area. China is ranked first in the world in terms of population (143,880,000) living in low-lying coastal zones (McGranahan et al., 2007). As a highly urbanized and developed region in China, the Yangtze River Estuary is located in a low-lying area and is thus sensitive to typhoons. Therefore, the hazards of typhoon-induced storm surge and waves must be quantified to provide more information to assist efforts to plan for and design future development strategies to reduce the loss and destruction caused by storms.

Because of the climate change and irreversible impacts of human activities, sea level rise (SLR) has become a crucial environmental topic worldwide. Zhou et al. (2013) pointed out that the relative SLR could range from 1.54 m to 2.7 m within the Yangtze River Estuary by the end of the 21st century when considering land subsidence. As one of China's economic centers, Shanghai, together with its adjacent regions, is expected to suffer substantial loss from disasters such as coastal erosion and hydrodynamic environmental changes caused by SLR. Zhou et al. (2013) also indicated that significant topographic changes could occur under SLR above 0.59 m during the wet season. Together with the associated increases in current velocity, the northern coasts of the Yangtze River Estuary could suffer from the effects of severe beach erosion. Kuang et al. (2014) found significantly increased tidal levels in the Yangtze River Estuary and demonstrated that the related rate of increase gradually decreases upstream along the channel. Moreover, the ebb flow split ratio in the North Branch may be as high as 5% under the SLR scenario.

Recent studies have focused on the impacts of future SLR on storm surge and waves. Zhao et al. (2014) applied

Received June 8, 2018; accepted November 26, 2018

E-mail: ymshen@dlut.edu.cn

a coupled model based on the simulation of waves nearshore (SWAN) and advanced CIRCulation (ADCIRC) to determine the possible effects of SLR on storm surges within the Yangtze River Estuary. Given the bottom roughness change caused by SLR was neglected, this study indicated a weakly sensitive relationship between extreme surges and SLR. Another wave model, STWAVE, was fully coupled with ADCIRC and applied to investigate the impacts of 0.5 and 1.0 m SLRs on storm surge and waves around the regions of southeast Louisiana (Smith et al., 2010). The results of this work showed that surge propagation in shallow water systems is highly sensitive to SLR. Bilskie et al. (2014) demonstrated that the response of storm surges to SLR is nonlinear, which is in contrast to the linear relationship proposed by Yang et al. (2015). This difference may be attributed to variations in the related study regions and typhoon cases.

Nearly the entire Yangtze Delta is protected by seawalls. These structures may explain why the associated coastal inundation (CI) is often neglected in many studies concerning SLR within the Yangtze River Estuary. However, the usability of these seawalls in future SLR cases cannot be guaranteed. Moreover, applying flooding areas to the current models could induce major differences among the results obtained. Pelling et al. (2013) found that the decision of whether or not to adopt flood defences in the model used to simulate tidal processes under the SLR case can lead to different results. Under flooding conditions, the amplitudes of M2 could change by up to 20 cm in some regions around Bohai Sea relative to the result of the no-flooding condition. Consequently, the impacts of WDI and CI induced by SLR on storm surge and waves must be further studied. The purpose of this paper is to: (i) analyze the impact of two key environmental factors, namely, WDI and CI, induced by SLR on storm surge and waves; (ii) analyze the interaction between WDI and CI; and (iii) provide practical suggestions on the adoption or neglect of CI in future related research and infrastructure design. Herein, a 1.0 m SLR is chosen based on its likelihood of occurrence over the next 50–100 years (Cheng et al., 2018).

2 Numerical model description

The FVCOM model developed by Chen et al. (2003, 2007), and has been widely applied to hydrodynamic simulations, can simulate tides, flooding, storm surges, and material diffusion. To solve the related three-dimensional primitive equations, FVCOM uses the finite-volume approach to ensure better conservation of mass and momentum. It also uses triangular mesh in the horizontal plane and applies a sigma coordinate in the vertical direction to enable easy capture of meandering shorelines and rough seabed shapes. The coefficient of vertical mixing is calculated by the Mellor–Yamada 2.5 turbulence closure (Mellor and Yamada, 1982). The mode separation method, together with the point drying/wetting treatment implemented by FVCOM, significantly increases the computational efficiency and stability.

The SWAN model developed by Delft University of Technology (Netherlands) is used to obtain wave parameters in aquatic regions, such as tidal inlets and estuaries (Deltares, 2013). This model is based on the balanced equation of discrete spectral action (Hasselmann et al., 1973). Transformation from the primitive structured grid version to an unstructured grid version was performed to fully couple the model with FVCOM. The fully coupled current-wave module in FVCOM plays an important role in simulating hydrodynamics under various conditions, such as current, tides, and typhoon-induced storms, among others.

3 Model setup and verification

3.1 Typhoon model

3.1.1 Typhoon selection

Typhoon Haikui (1211) formed as a tropical depression above the northwestern Pacific Ocean on 3 August 2012 (Fig. 1(c)). It then moved to the western region of China with increasing speed and intensity. On 5 August, it intensified into a tropical storm with a central pressure of 965 hPa and a maximum wind speed of approximately 50 m/s. Haikui eventually made landfall in the coastal region of Hepu Town, Xiangshan City, Zhejiang Province at 03:00 pm (Beijing time) on August 7. Due to the typhoon's extreme speed, large scale, and low pressure, the region's coastal zones experienced extensive damage. Detailed information on this typhoon, such as its central location, velocity, and pressure, can be obtained from the Chinese typhoon weather website.

3.1.2 Typhoon model description

Accurate modelling of storm surge and wave characteristics is closely related to the accuracy of the typhoon model. Therefore, applying a precise atmospheric pressure and wind field formula is a basic and key precondition in typhoon simulation. Several parametric equations with reasonable parameter settings have been adopted to produce accurate models. The following empirical formula is adopted to calculate the radius of maximum wind speed (Yin et al., 2016):

$$R_{\max} = 28.52\tanh[0.0873(\varphi - 28)] + 12.22\exp\left(\frac{P_c - 1013.25}{33.86}\right) + 0.2C + M, \quad (1)$$

where R_{max} presents the radius of the maximum wind speed, φ presents the latitude of the typhoon center (deg), M presents the initial radius, P_c presents the cyclone center pressure, and C presents the speed of the cyclone center.

According to relevant research on typhoon simulations around the East China Sea, the improved Holland–B formula is applied to calculate the pressure and wind field for the present model, expressed as follows (Holland, 1980, 2008):

$$P(r) = P_c + (P_n - P_c)(-R_{max}/r)^B, \tag{2}$$

$$V(r) = \sqrt{(P_n - P_c)\frac{B}{\rho_a}\left(\frac{R_{max}}{r}\right)^B \exp\left(-\frac{R_{max}}{r}\right)^B + \left(\frac{rf}{2}\right)^2} - \frac{rf}{2}, \tag{3}$$

where $P(r)$ presents the pressure at a distance r from the typhoon center, P_n is the ambient pressure with a constant value of 1013 hPa, r presents the distance from the typhoon center to the calculation point, $V(r)$ presents the velocity at a distance r from the typhoon center, f presents the Coriolis force parameter, and B represents an index that affects the kurtosis and intensity of a typhoon, given by the following formula (Vickery et al., 2000):

$$B = 1.881 - 0.00557R_{max} - 0.01295\varphi. \tag{4}$$

To enhance the accuracy of the typhoon model, the pressure and wind field obtained from the Cross Calibrated Multi-Platform (CCMP) is applied as a background field to provide asymmetry and values of the far-typhoon-center region to the theoretical field. The combined method is expressed as follows (Hubbert et al., 1991):

$$K(r) = [1 - e(r)]K_h(r) + e(r)K_c(r), \tag{5}$$

$$e(r) = m(r)^4/[1 + m(r)^4], \tag{6}$$

$$m(r) = r/(9.5R_{max}), \tag{7}$$

where $K(r)$ is the value of interest (pressure or wind velocity) at a distance r from the typhoon center, K_h is the value of interest obtained from the Holland formula, K_c is the value of interest obtained from CCMP, and $e(r)$ is the blend coefficient.

3.2 Tidal current model

3.2.1 Model domain and mesh

Hydrodynamic processes within the Yangtze River Estuary are relatively complicated because of the wide distribution of islands and numerous river outlets; therefore, the interactions between tides, waves, and river discharges must be considered. To accurately reproduce the hydrodynamic characteristics in the area of interest, a high-precision model is desired. An outer boundary far from the area of interest was selected to ignore the boundary wave inputs in the typhoon modelling process. The model domain is illustrated in Fig. 1(a). The computational

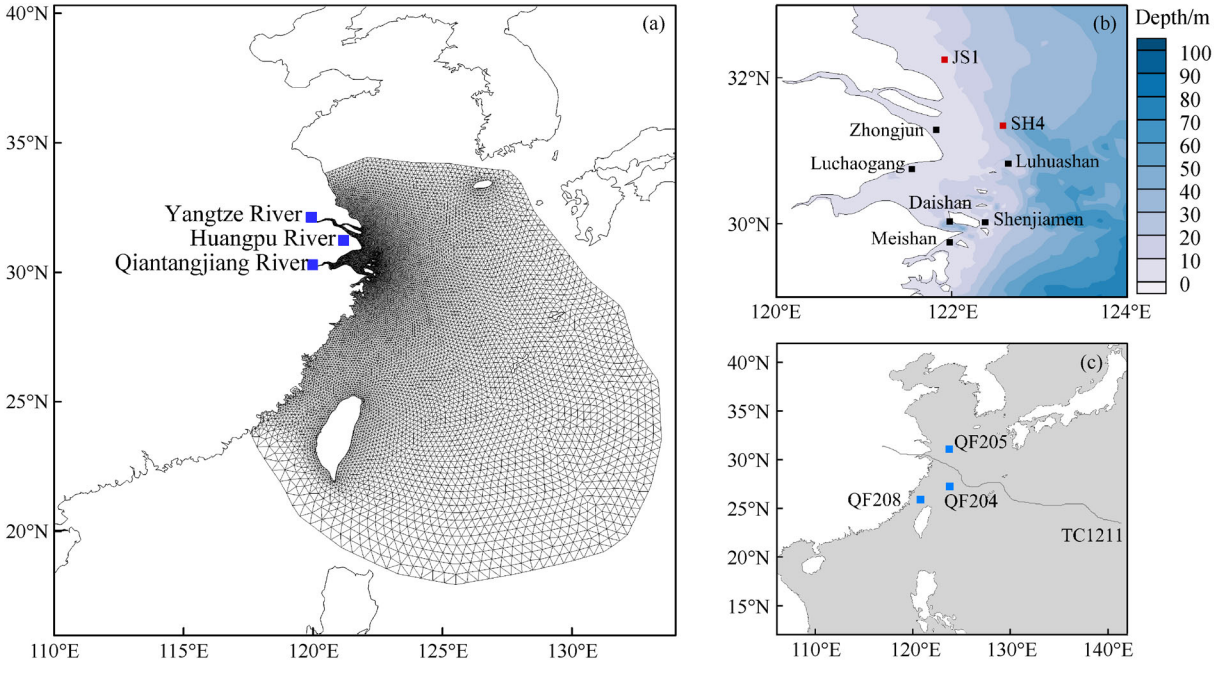

Fig. 1 Model information. (a) Triangular mesh in the study domain; (b) topography and verification stations within the Yangtze River Estuary; (c) track and verification stations of typhoon Haikui.

domain covers not only the whole region of the Yangtze River Estuary, but also a major portion of the East China Sea. This model domain is confined in the north by 33.8°N, the south by 17.5°N, and has an extensive span of 117.8°E–132.8°E in longitude.

A rough triangular mesh and a high-resolution mesh in the area of interest are applied to balance the accuracy and efficiency of simulations. This tidal current model has 12,105 nodes and 24,506 elements, with an extensive grid size of 5 km in the open boundary and a narrow grid size of about 100 m near the Yangtze River Estuary. A global topography database, ETOPO2, is used for bathymetry interpolation in most of the domain except for the Yangtze River Estuary, where the bathymetry is acquired from higher-resolution field measurements.

3.2.2 Initial and boundary conditions

The tidal current model starts with zero flow velocity and mean sea level (MSL). Coastlines are treated as closing boundaries with no-flow conditions. The Yangtze, Huangpu, and Qiantangjiang Rivers are set as river discharge inputs, with their monthly average discharges used according to the multi-year database analysis. Along the open-sea boundary, the time series of water levels are adopted by combining four main tidal constituents (M2, S2, K1, and O1) with four minor constituents (N2, K2, Q2, and P1). Atmospheric forcing, including wind speed, is imposed on the model as a surface boundary condition. Data for this task are obtained from the European Centre for Medium-Range Weather Forecasts database with a resolution of 0.75° × 0.75°.

3.2.3 Parameter settings

Simulations begin at 00:00 (Beijing time), June 1, 2005 and ended at 00:00, 31 July 2005, using a 5 s time step for the internal mode and a 30 s time step for the external mode. Bottom roughness coefficients applied to this model are considered as spatially variable values changing from 0.01 to 0.002 based on different levels of local depth. For depths less than 10 m, 10–25 m, and above 25 m, the bottom roughness coefficients are 0.01, 0.007, and 0.002, respectively. To ensure the accuracy of simulation, a point drying/wetting treatment is applied to the model with a minimum depth of 0.05 m. In this treatment, an element is locked and cannot be used for calculation when its depth is less than 0.05 m.

3.2.4 Model verification

To assess the simulation accuracy of the model, the observation data and modelling results from 00:00, 10 July 2005 to 00:00, 14 July 2005 are compared. Six stations, Zhongjun, Luhuashan, Daishan, Shenjiamen, Meishan, and Luchaogang, are chosen to conduct comparisons at the tidal level (Fig. 1(b)). As shown in Fig. 2, tidal levels obtained from the simulation are in good agreement with the real-time data in terms of tidal range and phase. The root mean square errors between the modelling results and observations at Zhongjun, Luhuashan, Daishan, Shenjiamen, Meishan, and Luchaogang are 0.17, 0.18, 0.12, 0.09, 0.10, and 0.13 m, respectively, and the corresponding correlation coefficients are approximately 0.91, 0.89, 0.94, 0.92, 0.95, and 0.93. The simulation values of high tide in

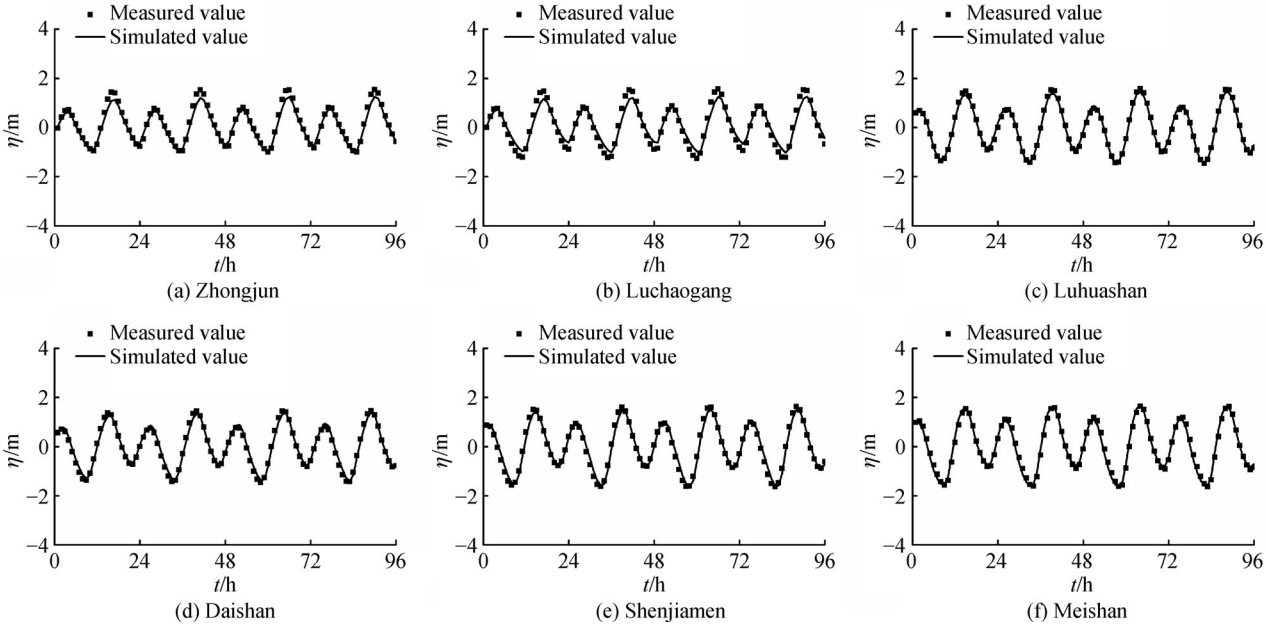

Fig. 2 Comparison between simulated and observed tidal levels at various stations (comparison begins at 00:00 on July 10, 2005). (a) Zhongjun; (b) Luchaogang; (c) Luhuashan; (d) Daishan; (e) Shenjiamen; (f) Meishan.

Zhongjun and Luchaogang do not match the measured values very well, likely due to the depth deviations when the measured depths are interpolated to near-shore regions. Two stations, JS1 and SH4, are chosen to perform comparisons of current velocity and current direction. As shown in Fig. 3, the modelling results agree well with the observed data. Thus, storm surges can be well reproduced by precise simulation of the tidal process.

3.3 Storm surge and wave model

3.3.1 Model setup

The computational mesh used in the storm surge model is identical to that used in the tidal model. From 00:00, August 1, 2012 to 00:00, August 10, 2012, modelling of storm surge and waves during typhoon Haikui is executed using a time step of 1 s for the coupled current-wave module. However, the river discharges during the typhoon are not available; thus, the estimated river runoffs applied to the tidal model are used in the typhoon modelling process. The sensitivity of the river discharge is evaluated, and no important influence on the simulations is found. Other parameters, such as bottom roughness coefficient, are set as those applied to the tidal model. Parameters for waves, which are not included in the former model, are configured based on related research (Jia et al., 2018). The JONSWAP empirical model is used to acquire the bottom friction with a friction coefficient of approximately 0.067 $m^2 \cdot s^{-2}$ (Yin et al., 2017).

3.3.2 Wave height verification

Due to the lack of real-time data for wave heights in offshore areas during typhoon Haikui, three stations in the East China Sea with depths of more than 50 m and offshore distances of more than 2 km are used as verification stations (Fig. 1(c)). Using data obtained from these stations, verifications of wave height are carried out over the period beginning at 16:00 on August 5 (Fig. 4). Among these stations, QF204 recorded the maximum wave height owing to its proximity to the typhoon center trace whereas QF205 showed a delay in the time for maximum wave height appearance owing to its farthest distance from the

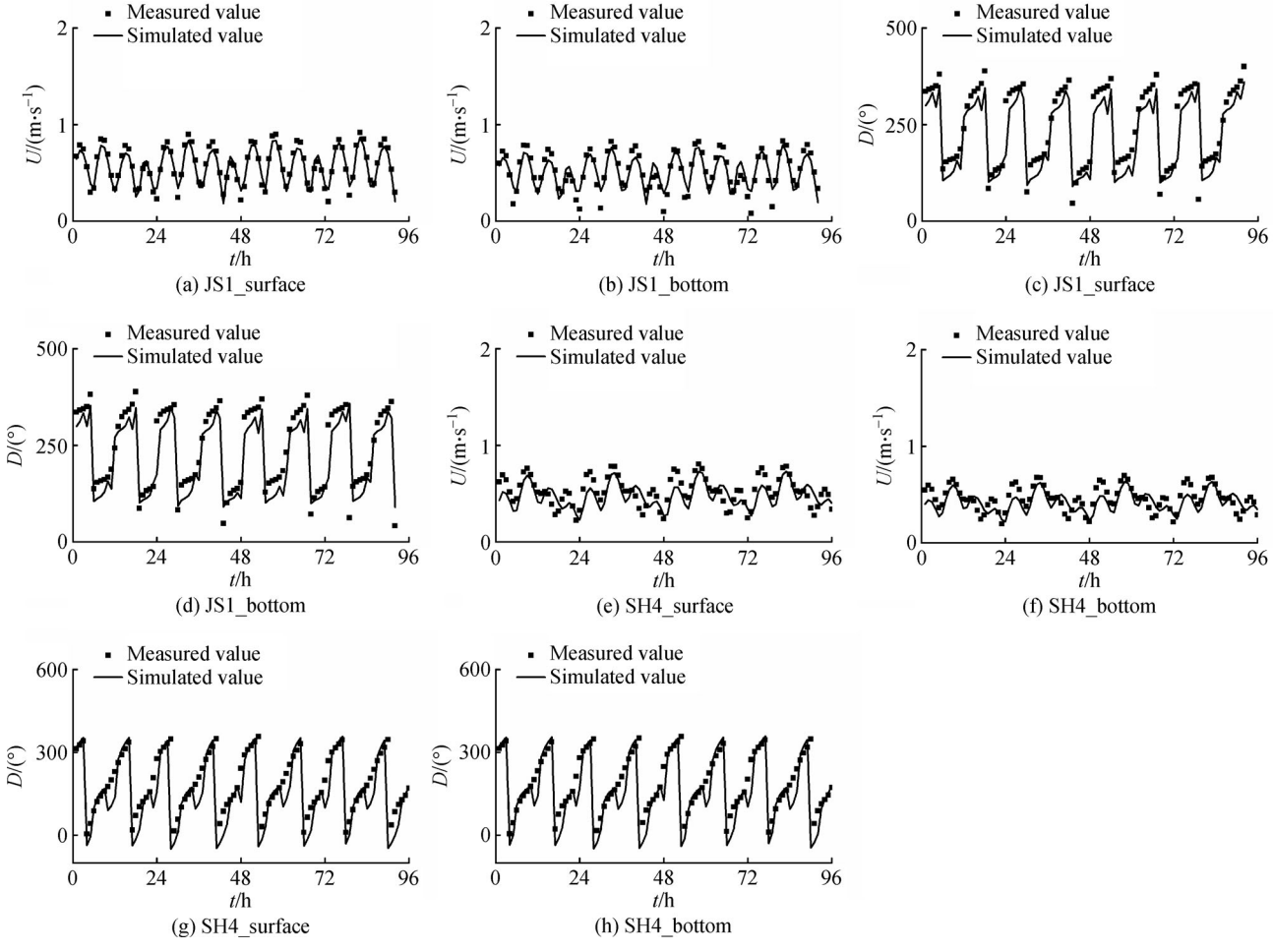

Fig. 3 Comparison between simulated and observed tidal currents at JS1 station (a–d) and SH4 station (e–h) (comparison begins at 00:00 on July 10, 2005).

typhoon center trace. Verification results indicate that the simulated predictions of typhoon Haikui are consistent with the observations recorded at these stations.

4 Coastal inundation induced by SLR

To obtain the CI caused by SLR, the topography around the region of interest is strongly desired (Wang et al., 2012). A general strategy to find the new coastline can be expressed by subtracting the value of SLR from the current topography of the surface. Herein, the current topography of the region of interest is subtracted by the 1.0 m SLR, resulting in the new topography. Based on this calculation, the newly derived topography is determined to be above zero, indicating that the region of interest is the mainland whereas other areas comprise the ocean. Software developers have recently developed an Android mobile phone application called Elevation Earth that presents inundations under different magnitudes of SLRs. Figure 5 presents the coastlines in different SLR cases ranging from 1.0 m to 3.0 m clearly indicating that Shanghai City and Hangzhou City could potentially disappear under SLR. Consistent with expectations, the Yangtze River Delta appears to be more sensitive to SLR compared with other regions owing to its low terrain caused by sediment accumulation.

The applicability of inundated coastlines derived from this method to the former model must be illustrated. The topography in Elevation Earth is based on Google Earth data, which do not conform to measurements applied in the former model. Therefore, direct use without pre-processing could cause potential errors. The assumption that the sensitivity of a coastal area to SLR is constant in different databases is proposed under this data-limited condition. Taking land sensitivity into consideration is logical when the extracted coastlines are not applied. Figure 6 presents the inundated area within the Yangtze River Estuary under a 1.0 m SLR.

In reality, nearly all of the Yangtze River Delta is protected by seawalls. The existing seawalls are capable of coping with floods that have a 20-year recurrence interval. Thus, a 1.0 m SLR may not result in serious inundation. The data used in Elevation Earth are more natural and include a few seawalls and other facilities, thereby leading to an obvious inundated condition. However, the usability of these seawalls under future SLR cases cannot be guaranteed. In addition, the impact of CI without seawall protection may cause major differences among the results obtained. Therefore, in this data-limited condition, the inundation process can be reasonable and scientifically valuable to some extent. Application of CI enables investigation of its effects and the combined effects (WDI and CI) on the storm process, which are often ignored in many related studies.

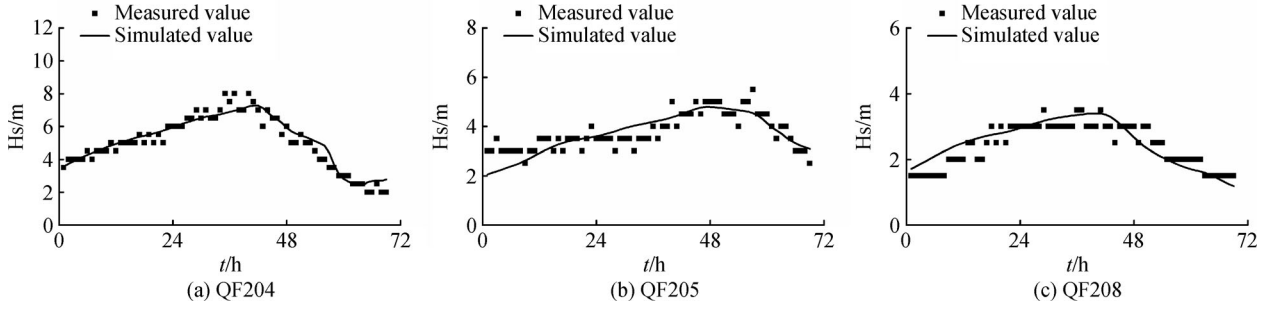

Fig. 4 Comparison between simulated and observed wave height at (a) QF 204; (b) QF 205; (c) QF 208 stations during typhoon Haikui (comparison begins at 16:00 on August 5, 2012).

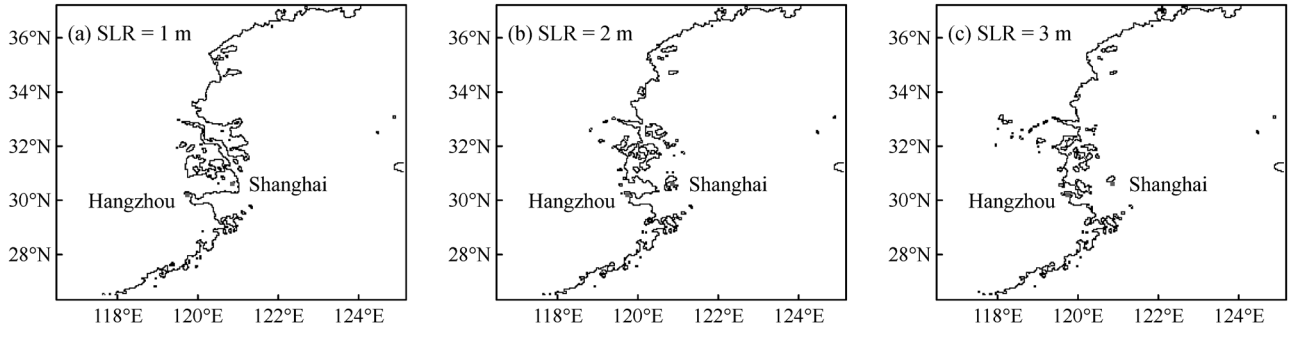

Fig. 5 Coastal inundation induced by SLR. (a) 1.0 m SLR; (b) 2.0 m SLR; (c) 3.0 m SLR.

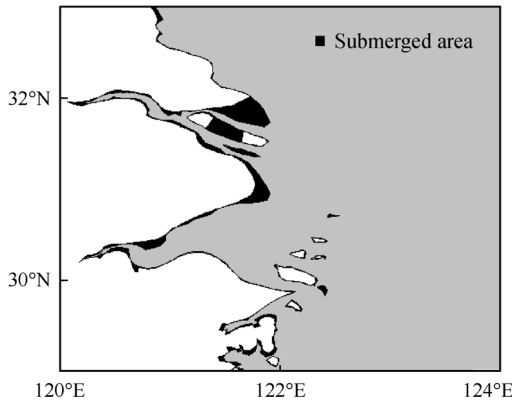

Fig. 6 Coastal inundation induced by 1.0 m SLR within the Yangtze River Estuary.

5 Effects of WDI and CI, induced by SLR, on storm surge and waves within the Yangtze River Estuary

The potential effects of WDI and CI induced by a 1.0 m SLR on storm surge and waves within the Yangtze River Estuary are explored using the validated-coupled current-wave module. Vegetation type and land subsidence caused by SLR are not considered in this simulation (Passeri et al., 2015; Wang et al., 2018). Four scenarios are configured with the different water depths and coastlines (Table 1). Eight tidal constituents described at the open boundary remain the same among the different scenarios. The SLR is achieved by adding 1.0 m water depth to the present water depth, thus increasing the MSL by 1.0 m. To investigate the effects of CI, the newly inundated coastline obtained from Fig. 6 is applied to the related scenarios (S3, S4). Bottom roughness coefficients are updated according to the new water depth with the same coefficient span described in Section 3.1.3, whilst other parameters are kept identical to those in the storm surge model (Yin et al., 2017). The additional submerged regions in S3 and S4 are different. For S3, where the original water depth is applied, the additional area is dry. This case is similar to the flooding case, and the bottom roughness coefficient is set to the maximum (0.01) in the newly submerged area. For S4, the additional area is filled with water, and the bottom roughness coefficient is calculated based on the new water depth.

The MSL actually changes with different scenarios. The MSL is 0 m in S1 and S3, where the water depth equals the original value, and 1.0 m in S2 and S4 owing to the 1.0 m WDI applied. Calculations of storm surges and wave heights are referenced to the MSL. To eliminate the effect of the MSL, the surges among these four scenarios are acquired from the difference between the tidal elevation in the storm surge model and those in the modelling wherein only astronomical tide is considered. The water depth in the two models is kept constant. Therefore, the differences in storm surges and wave heights among the scenarios do not include the SLR. A positive value means the increase in water level is greater than the SLR, whereas a negative value indicates the increase is smaller than the SLR. Differences among the results of the four scenarios reflect the effect of factors on storm surge and waves together with the relationship between the two factors. The effects of WDI and CI, the combined effects of both factors, and the strength of their influences and linear relationship are of great concern. The processing methods of these subjects are illustrated in Table 2.

Table 1 Scenario configuration

Scenario name	Water depth	Coastal line
Scenario 1 (S1)	Original water depth	Basic coast
Scenario 2 (S2)	1.0 m WDI	Basic coast
Scenario 3 (S3)	Original water depth	Inundated coast
Scenario 4 (S4)	1.0 m WDI	Inundated coast

Table 2 Description and explanation of results processing

Results processing	Description	Explanation
S2 − S1	Single factor effect (WDI)	Absolute value presents the strength while symbol presents the change tendency
S3 − S1	Single factor effect (CI)	Absolute value presents the strength while symbol presents the change tendency
S4 − S1	Combined effect (WDI and CI)	Absolute value presents the strength while symbol presents the change tendency
|S2 − S1| − |S3 − S1|	Compare the strength between the two factors	Difference above zero implies the stronger effect of WDI than CI
S4 − S3 − S2 + S1	Quantify the linear relationship between the two factors	Difference near zero implies a better linear relationship between the two factors

5.1 Effects on storm surges

To illustrate how WDI and CI affect the storm surge, maximum storm surges among scenarios are shown in Table 3. In general, WDI and CI do not have a substantial impact on the amplification of maximum storm surges under a 1.0 m SLR. A 1.0 m WDI decreases the maximum storm surge by 0.15 m, thus weakening the maximum surge. This negative effect is consistent with the result of previous studies and may be caused by the reduction in bottom friction due to deep water levels during SLR (Gao et al., 2008; Bilskie et al., 2014; Zhao et al., 2014; Yin et al., 2017). This amplification is similar to that simulated in the study of Yin et al. (2017) (0.13 m). However, this effect of WDI on storm surge contrasts with that found by Smith et al. (2010) and may be attributed to differences in vegetation. Unlike the Yangtze River Estuary, the topography of the southeast region of Louisiana consists of many marshes. Consequently, substantial changes in the Manning coefficient are obtained with increasing water depth. CI slightly decreases the maximum surge by 0.04 m, which is smaller than that induced by WDI. The inundated coastline is wider in comparison with the basic coastline. Therefore, with more land surface, water volume accumulation around the shallow area during a typhoon decreases, resulting in a lower maximum storm surges than observed in the basic scenario. Nevertheless, this boundary effect on storm surges under the 1.0 m SLR case is limited. The combined effect of WDI and CI significantly decreases the maximum surge by 0.31 m. Strength comparison between factors shows that WDI is primarily responsible for the observed decrease in the maximum storm surge. The combined effects of WDI and CI greatly exceed individual effects, which means the relationship between WDI and CI is highly nonlinear, and thus their combined effect is more extensive than either of the single-factor effects.

Figure 7 presents the spatial distribution of the maximum storm surges within the Yangtze River Estuary

Table 3 Maximum storm surge and maximum significant wave height in four scenarios

Scenario name	Maximum storm surge/m	Maximum significant wave height/m
S1	3.13	8.30
S2	2.98	8.65
S3	3.09	8.23
S4	2.82	8.51

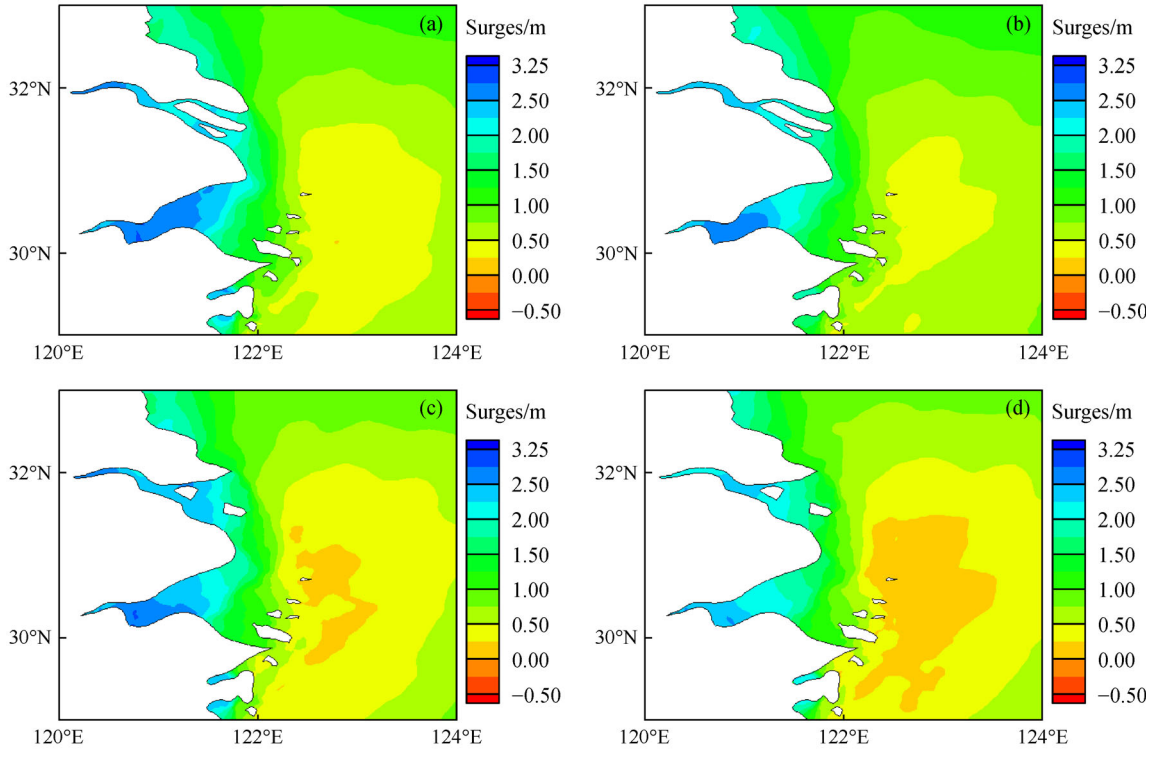

Fig. 7 Distribution of maximum storm surges within the Yangtze River Estuary. (a) Basic scenario S1; (b) 1.0 m WDI scenario S2; (c) CI scenario S3; (d) 1.0 m WDI and CI scenario S4.

among the four scenarios. These scenarios generally show similar spatial distributions of maximum storm surges. Hangzhou Bay and Yangtze River Estuary reveal superior storm surges compared with those observed in other deep-water areas, with a gradual increase observed in maximum storm surges upstream along the channel. As shown in related research (Zhao et al., 2014), this distribution may be caused by the shallow water condition and narrow coastline restriction, which aide in the accumulation of water. The storm surges are higher along Hangzhou Bay than along the Yangtze River Estuary because of the selected typhoon track, which is adjacent to the former. The effect of WDI and CI induced by 1.0 m SLR does not remarkably influence this spatial distribution.

To determine how the factors interact to influence the maximum storm surges, strength comparison and linear relationship analyses are conducted. Figure 8(a) presents a strength comparison between WDI and CI. Values above zero imply the stronger effect of WDI, while values below zero indicate the stronger effect of CI. In near-shore areas, WDI and CI exhibit strong effects. The strong effect of WDI is caused by the relatively significant water depth increase that significantly alters the local hydrodynamic environment, thereby stimulating changes in maximum storm surges. Meanwhile, these low-lying regions suffer from inundation, with a significant effect of CI. However, in deep-water areas where the relative change in water depth is minimal, the effect of CI is gradually enhanced. In most deep-water areas, values of the strength comparison are consistently small. This finding indicates the weak effect of WDI and CI in the deep-water areas due to the great depth and long distance from the inundated area. Figure 8(b) presents the linear relationship between WDI and CI, where the minimal value in the difference between the surges indicates a good linear relationship. As expected, near-shore areas often show a higher difference in value than observed for deep-water areas. Because of the shallow water and variations in coastline in near-shore areas, the contributions of WDI and CI are significant, and their combined effects are more extensive than that of either of the single factors. This finding reveals a nonlinear relationship between WDI and CI around the near-shore areas. However, in deep-water areas, the linear relationship emerges owing to the weak effect of the two factors.

To better understand the effects of WDI and CI on storm surges, three paths were selected for comparison: Tracing Path A: North Branch of Yangtze River Estuary; Tracing Path B: the area between the North and South Channels of the Yangtze River Estuary; and Tracing Path C: the Hangzhou Bay (Fig. 9). Figure 10 shows the storm surges (not the maximum surges) at a specific time along these tracing paths in four scenarios. As expected, the surges decrease downstream along these three paths, and inner areas show higher storm surges than in the outer areas

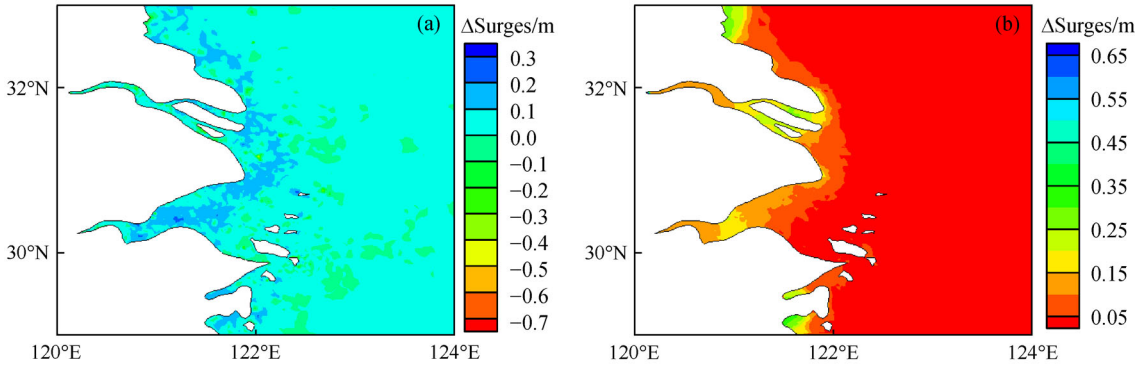

Fig. 8 Strength comparison and linear relationship between the effect of WDI and CI on maximum storm surges within the Yangtze River Estuary. (a) Strength comparison, Δsurges = |surges in S2 − surges in S1| − |surges in S3 − surges in S1|; (b) linear relationship, Δsurges = surges in S4 − surges in S3 − surges in S2 + surges in S1.

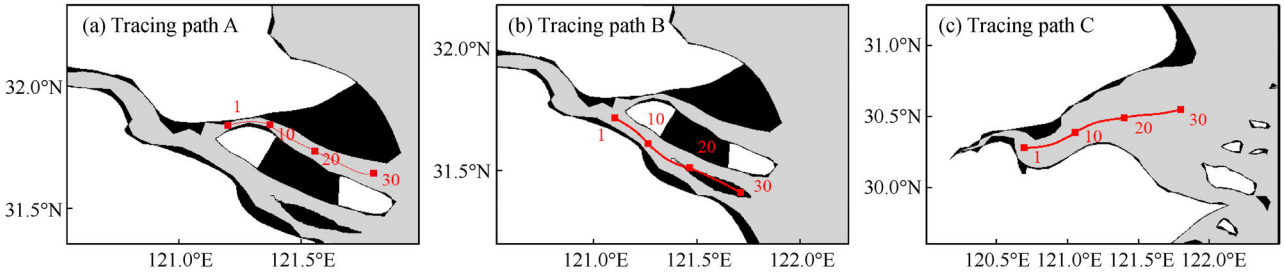

Fig. 9 Sketch map of the three tracing paths. (a) Points along tracing path A; (b) points along tracing path B; (c) points along tracing path C.

connected to the ocean as shown in Figs. 10(a), 10(d), and 10(g). Figures 10(b), 10(e), and 10(h) present the effects of WDI, CI, and their combination. WDI plays a negative role around inner areas, but plays a positive role around outer areas. In inner areas, where the water depth is shallow, a 1.0 m WDI can cause significant hydrodynamic changes, which, together with the reduced bottom roughness coefficient, could lead to the decrease in storm surge. However, in outer areas, a 1.0 m WDI slightly increases the storm surges. CI largely changes surges in the near-shore areas that experience massive CI, but in other deep-water regions, its effect is less. The linear relationship of WDI and CI is shown in Figs. 10(c), 10(f), and 10(i). Because of minimal coastline changes and its wider shape, Hangzhou Bay shows a better linear relationship between WDI and CI than in the Yangtze River Estuary (the two lines are close to each other in Fig. 10(i)). For the Yangtze River Estuary, the separation between the lines is greater, which indicates a nonlinear relationship.

5.2 Effects on waves

The maximum significant wave heights during the storm period in the study domain were selected to show the effects of WDI and CI on waves that were induced by 1.0 m SLR. The maximum significant wave heights of the four scenarios are presented in Table 3. Generally speaking, the variation in wave height is more substantive than that in storm surge. A 1.0 m WDI increases the maximum wave height by 0.35 m. This amplification is dissimilar to that simulated in the study of Yin et al. (2017) (0.46 m), and could be attributed to differences in the characteristics of the typhoons simulated. By contrast, CI decreases the maximum significant wave height by 0.07 m, which may be caused by the additional inundated area in S3, which releases wave energy during flooding. The combined effect of WDI and CI increases the maximum significant wave height by 0.21 m. This increase is smaller than the WDI primarily caused by the opposing influences of the two

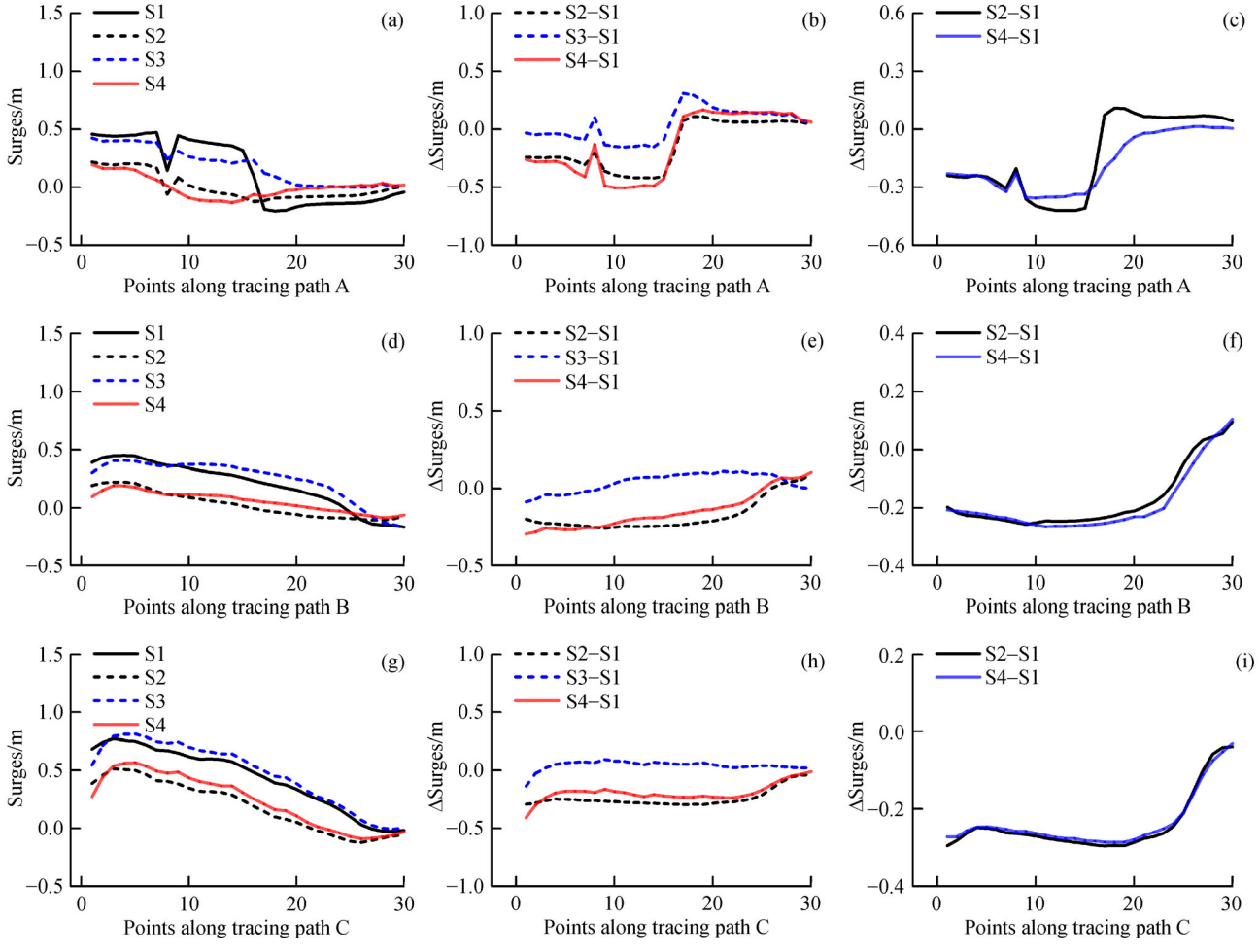

Fig. 10 Storm surges along the three tracing paths in four scenarios and their relationships. The first column (a, d, g): storm surges along paths in four scenarios; the second column (b, e, h): effects of WDI, CI and the combined factors; the third column (c, f, i): linear relationship between WDI and CI.

factors. Strength comparison between factors shows that WDI is mainly responsible for the significant wave height increase observed.

The spatial distributions of the maximum significant wave height within the Yangtze River Estuary in four scenarios are presented in Fig. 11. The four scenarios generally show similar spatial distributions of maximum significant wave height, except for the amplitude of the maximum value. The WDI and CI induced by 1.0 m SLR do not remarkably alter this spatial distribution. The two key factors affecting the significant wave height are water depth and wind velocity. Therefore, regions belonging to the open sea tend to have a higher wave height than bodies of water primarily surrounded by land. In addition, areas close to the typhoon track reveal higher wave heights than those away from typhoon threats.

To determine how the factors interact and influence the maximum significant wave height, strength comparison and linear relationship analyses are conducted. Figure 12(a) presents a strength comparison between WDI and CI. In near-shore areas, where the depth-limited breaking is important, larger water depths induced by WDI signifi-

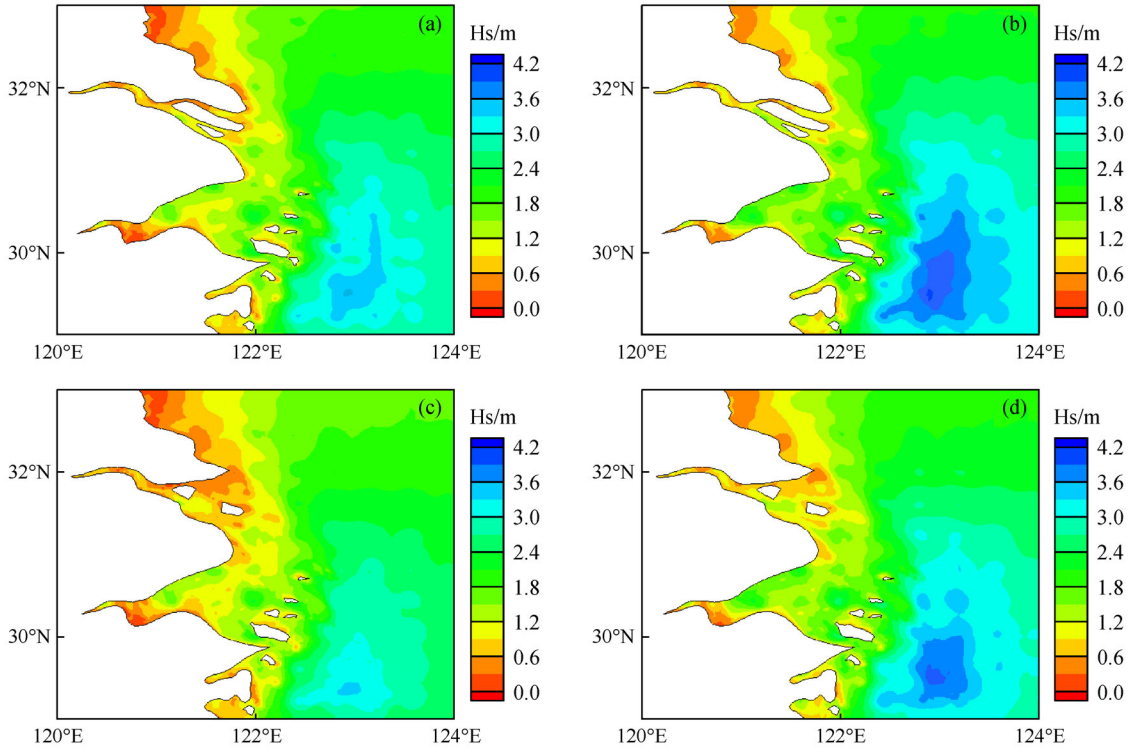

Fig. 11 Distribution of maximum significant wave heights within the Yangtze River Estuary. (a) Basic scenario S1; (b) 1.0 m WDI scenario S2; (c) CI scenario S3; (d) 1.0 m WDI and CI scenario S4.

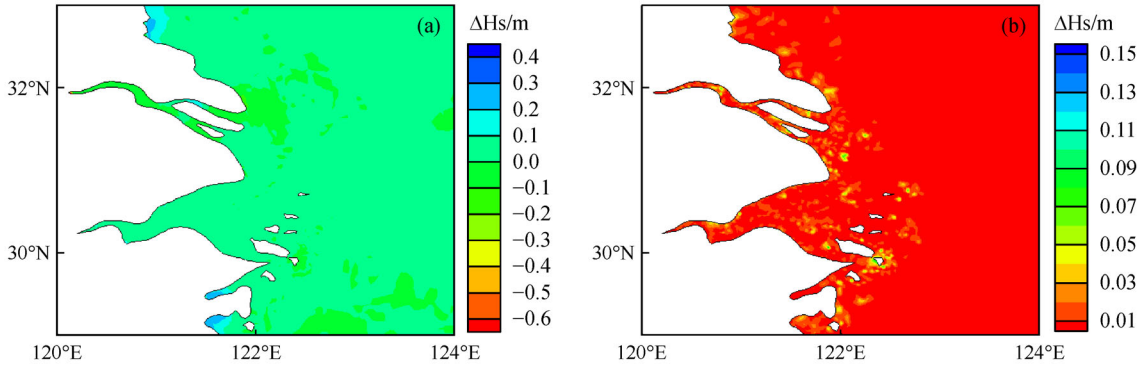

Fig. 12 Strength comparison and linear relationship between the effect of WDI and CI on maximum significant wave heights (Hs) within the Yangtze River Estuary. (a) Strength comparison, ΔHs = | Hs in S2 − Hs in S1| − | Hs in S3 − Hs in S1|; (b) linear relationship, ΔHs = Hs in S4 − Hs in S3 − Hs in S2 + Hs in S1.

cantly change the depth-limited breaking and increase the maximum significant wave heights. Low-lying regions are vulnerable to inundation resulting in significant effects on CI. In deep-water areas, where the relative change in water depth is minimal, the effect of CI is gradually enhanced. However, values of the strength comparison are always small. This finding indicates the weak effect of WDI and CI around the deep-water areas owing to the long distance from inundated areas and the water depth. Figure 12(b) presents the linear relationship between WDI and CI. Similar to the discussion on maximum storm surges, deep-water areas show a better linear relationship between WDI and CI than near-shore regions.

To better understand the effect of WDI and CI on waves, Fig. 13 presents the distribution of significant wave heights (not the maximum wave height) at a specific time along the three tracing paths. Change patterns in the four scenarios are similar along these paths. Significant wave height, primarily caused by depth-limited breaking, increases downstream. Given Hangzhou Bay is located close to the typhoon track, it has a higher wave height than the Yangtze River Estuary. Figures 13(b), 13(e), and 13(h) present the effects of WDI, CI, and their combination. WDI plays a positive role among the four scenarios. The effect of CI is consistently minimal, but becomes significant when the surrounding coastline is extensively altered. Meanwhile, around the inundated areas, the combined effects of WDI and CI exceed their individual effects. Therefore, the impact of CI should not be neglected in studies related to wave height simulations. The linear relationship between WDI and CI is shown in Figs. 13(c), 13(f), and 13(i). Areas with slight coastline change tend to show a better linear relationship between WDI and CI than areas with large coastline changes. For inundated areas, the separation between lines is greater, indicating a nonlinear relationship caused by the stronger effect of CI. As expected, Hangzhou Bay shows a better linear relationship between WDI and CI than the Yangtze River Estuary due to minimal coastline changes and its wider shape, which is similar to the discussion on storm surges.

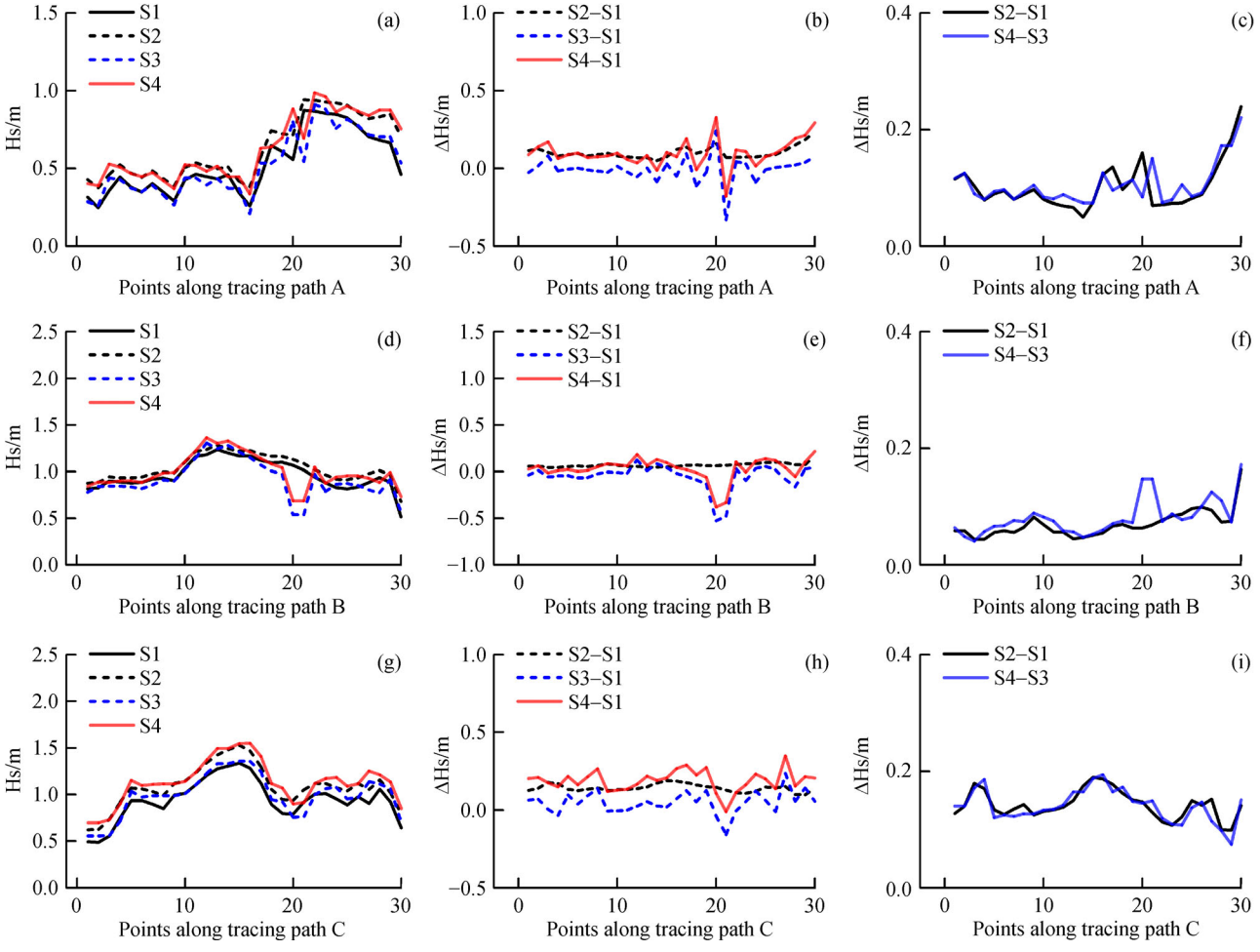

Fig. 13 Significant wave heights (Hs) along the three paths in four scenarios and their relationships. The first column shows significant wave heights along paths in four scenarios (a, d, g); second column shows the effects of WDI, CI, and the combined factors (b, e, h); and the third column shows the linear relationship between WDI and CI. (c, f, i).

5.3 Suggestions on the adoption or neglect of CI

The results of simulation (S4) with the compound factors of WDI and CI are different from those obtained from simulation (S2) wherein only WDI is considered. Compared with S2, the amplitudes of the maximum storm surges and wave heights in S4 tend to decrease (Table 3). Thus, for the design of infrastructures, such as offshore oil platforms and sea-crossing bridges which are fully- or partly-constructed in deep-water regions, neglecting CI is suggested when designing the maximum wave height. The maximum wave height is greater without CI which could increase standards in the construction of these infrastructures leading to a safer environment.

The spatial distribution of maximum storm surges and wave heights between S2 and S4 is similar (Figs. 7 and 11). However, in some low-lying areas and deep-water regions, major differences are observed. The water level is shallow in a newly submerged area, resulting in a higher tidal velocity and enhanced bed friction, thereby dissipating more energy. This effect shifts the amphidromic point to dissipation-enhanced locations and consequently alters the tidal characteristics in the deep-water region (Pelling and Mattias Green, 2013). Moreover, this effect varies with the local depth and surrounding hydrodynamic environment. For studies concerning topics such as water age and water quality, which are sensitive to the hydrodynamic environment, adoption of CI is suggested to obtain a better understanding and forecasting ability.

Many developed cities have flood defence plans and seawalls to prevent potential hazards from SLR and typhoons. In addition, due to the significant strategic position and high-density population of a low-lying area, this region may experience huge loss during natural disasters. Thus, the setting of reasonable flood control standards and construction of seawalls is important. In the present work, storm surges and wave heights are different between S2 and S4 (Figs. 10 and 13) along the three tracing paths. Storm surges are higher in downstream regions than upstream regions when taking WDI and CI into consideration. These differences may be caused by the increases in tidal wave energy dissipation, as well as the alterations in tidal phase and modulation (Arns et al., 2015). Significant wave heights exhibit major differences around newly submerged areas because of the powerful effects of WDI and CI and their nonlinear relationships. The amplitudes of wave heights may decrease in the middle of the South Branch of the Yangtze River Estuary, but increase in the upstream region of Hangzhou Bay. Therefore, the most dangerous situation can be obtained among the maximum of the results between S2 and S4. In other words, for the design of infrastructures such as seawalls, simulations should be more circumspect. The effects of both adoption and neglect of CI should be simulated to obtain the best flood control standard and design parameters.

6 Conclusions

This paper describes a scenario-based simulation on the effects of SLR on storm surge and waves. With the consideration of WDI and CI induced by SLR, the effects of WDI and CI on storm surge and waves can be simulated and analyzed. The model-predicted influencing results can also provide suggestions on the adoption or the neglect of CI in the related research and the design of infrastructures, such as offshore oil platforms and seawalls. The main conclusions are presented as follows.

In terms of individual effects, 1.0 m WDI decreases the maximum storm surge by 0.15 m and increases the maximum significant wave height by 0.35 m. The effect of CI is smaller compared with the effect of WDI; specifically, CI decreases the maximum storm surge and significant wave height by 0.04 and 0.07 m, respectively. This decrease may be caused by the additional submerged area, which releases a large amount of wave energy when flooding. The combined effect of WDI and CI decreases the maximum surge by 0.31 m and increases the maximum significant wave height by 0.21 m.

The spatial distribution of maximum storm surges and wave heights does not change remarkably in simulations of the four scenarios. However, in some low-lying areas and deep-water regions, major differences could be observed. In the near-shore area, increases in water depth significantly change the local hydrodynamic environment and stimulate the alteration of maximum storm surges and wave heights. Low-lying regions obviously suffer from inundation, thus leading to a significant effect of CI. In deep-water areas where the relative change in water depth is minimal, the effect of CI is gradually enhanced. However, in most deep-water areas, differences in the strength comparison are always small revealing the weak effect of WDI and CI around the deep-water area which is primarily caused by the significant water depth and greater distance from the inundated land. This could also be the reason that the deep-water area shares a better linear relationship than coastal regions.

In the design of infrastructures, such as offshore oil platforms and sea-crossing bridges, constructed in the deep-water area, neglecting CI is suggested when designing the maximum wave height. For studies concerning topics such as water age and water quality, which are sensitive to the hydrodynamic environment, adoption of CI is suggested to achieve a better understanding and forecasting ability. For the design of infrastructures such as seawalls, simulations should be more circumspect. The effects of both adoption and neglect of CI should be simulated to obtain the best flood control standard and design parameters.

Acknowledgements This research was funded by the National Natural Science Foundation of China (Grant Nos. 51779039 and 51879028).

Reference

Arns A, Wahl T, Dangendorf S, Jensen J (2015). The impact of sea level rise on storm surge water levels in the northern part of the German Bight. Coast Eng, 96: 118–131

Bilskie M V, Hagen S C, Medeiros S C, Passeri D L (2014). Dynamics of sea level rise and coastal flooding on a changing landscape. Geophys Res Lett, 41(3): 927–934

Chen C, Huang H, Beardsley R C, Liu H, Xu Q, Cowles G (2007). A finite volume numerical approach for coastal ocean circulation studies: comparisons with finite difference models. J Geophys Res, 112(C3): C03018

Chen C, Liu H, Beardsley R C (2003). An unstructured, finite-volume, three-dimensional, primitive equation ocean model: application to coastal ocean and estuaries. J Atmos Ocean Technol, 20(1): 159–186

Cheng H Q, Chen J Y, Chen Z J, Ruan R L, Xu G Q, Zeng G, Zhu J R, Dai Z J, Chen X Y, Gu S H, Zhang X L, Wang H M (2018). Mapping sea level rise behavior in an estuarine delta system: a case study along the Shanghai coast. Engineering, 4(1): 156–163

Deltares (2013). Delft3D-WAVE User Mannel. Delft Hydraulics

Gao Z G, Han S Z, Liu K X, Zheng Y X, Yu H M (2008). Numerical simulation of the influence of mean sea level rise on typhoon storm surge in the East China Sea. Marine Science Bulletin, 10(2): 36–49

Hasselmann K, Barnett T P, Bouws E, Carlson H, Cartwright D E, Enke K, Ewing J A, Gienapp H, Hasselmann D E, Kruseman P, Meerburg A, Müller P, Olbers D J, Richter K, Sell W, Walden H (1973). Measurements of Wind-Wave Growth and Swell Decay during the Joint North Sea Wave Project (JONSWAP). Deutches Hydrographisches Institut

Holland G J (1980). An analytic model of the wind and pressure profiles in hurricanes. Mon Weather Rev, 108(8): 1212–1218

Holland G J (2008). A revised hurricane and pressure-wind model. Mon Weather Rev, 136(9): 3432–3445

Hubbert G F, Holland G J, Leslie L M, Manton M J (1991). A real-time system for forecasting tropical cyclone storm surges. Weather Forecast, 6(1): 86–97

Jia H, Shen Y M, Su M R, Yu C X (2018). Numerical simulation of hydrodynamic and water quality effects of shoreline changes in Bohai Bay. Front Earth Sci, 12(3): 625–639

Kuang C P, Chen W, Gu J, Zhu D Z, He L L, Huang H C (2014). Numerical assessment of the impacts of potential future sea-level rise on hydrodynamics of the Yangtze River Estuary, China. J Coast Res, 295(3): 586–597

McGranahan G, Balk D, Anderson B (2007). The rising tide: assessing the risks of climate change and human settlements in low elevation coastal zones. Environ Urban, 19(1): 17–37

Mellor G L, Yamada T (1982). Development of a turbulence closure model for geophysical fluid problems. Rev Geophys Space Phys, 20 (4): 851–875

Passeri D L, Hagen S C, Bilskie M V, Medeiros S C (2015). On the significance of incorporating shoreline changes for evaluating coastal hydrodynamics under sea level rise scenarios. Nat Hazards, 75(2): 1599–1617

Pelling H E, Mattias Green J A (2013). Sea level rise and tidal power plants in the Gulf of Maine. J Geophys Res Oceans, 118(6): 2863–2873

Pelling H E, Uehara K, Mattias Green J A (2013). The impact of rapid coastline changes and sea level rise on the tides in the Bohai Sea, China. J Geophys Res Oceans, 118(7): 3462–3472

Smith M K, Cialone M A, Wamsley T V, Mcalpin T O (2010). Potential impact of sea level rise on coastal surges in southeast Louisiana. Ocean Eng, 37(1): 37–47

Vickery P J, Skerlj P F, Steckley A C, Twisdale L A (2000). Hurricane wind field model for use in hurricane simulations. J Struct Eng, 126 (10): 1203–1221

Wang J, Yi S, Li M Y, Wang L, Song C C (2018). Effects of sea level rise, land subsidence, bathymetric change and typhoon tracks on storm flooding in the coastal areas of Shanghai. Sci Total Environ, 621: 228–234

Wang L, Zhao X D, Shen Y M (2012). Coupling hydrodynamic models with GIS for storm surge simulation: application to the Yangtze Estuary and the Hangzhou Bay, China. Front Earth Sci, 6(3): 261–275

Yang Z Q, Wang T P, Voisin N, Copping A (2015). Estuarine response to river flow and sea-level rise under future climate change and human development. Estuar Coast Shelf Sci, 156(1): 19–30

Yin K, Xu S D, Huang W R (2016). Modeling sediment concentration and transport induced by storm surge in Hengmen Eastern Access Channel. Nat Hazards, 82(1): 617–642

Yin K, Xu S D, Huang W R, Xie Y (2017). Effects of sea level rise and typhoon intensity on storm surge and waves in Pearl River Estuary. Ocean Eng, 136: 80–93

Zhao C J, Ge J Z, Ding P X (2014). Impact of sea level rise on storm surges around the Changjiang Estuary. J Coast Res, 68: 27–34

Zhou X Y, Zheng J H, Doong D J, Demirbilek Z (2013). Sea level rise along the East Asia and Chinese coasts and its role on the morphodynamic response of the Yangtze River Estuary. Ocean Eng, 71: 40–50